

# Complex biphase nature of the superconducting dome of the FeSe phase diagram

V. Svitlyk<sup>1\*</sup>, M. Raba<sup>2</sup>, V. Dmitriev<sup>3</sup>, P. Rodière<sup>2</sup>, P. Toulemonde<sup>2</sup>,  
D. Chernyshov<sup>3</sup>, M. Mezouar<sup>1</sup>

<sup>1</sup>ID27 High Pressure Beamline, European Synchrotron Radiation Facility, 38000, Grenoble, France

<sup>2</sup>Institut Néel, 38042, Grenoble, France

<sup>3</sup>Swiss-Norwegian Beamlines, European Synchrotron Radiation Facility, 38000, Grenoble, France

\*svitlyk@esrf.fr

## Abstract

Single crystal X-ray diffraction of synchrotron radiation as a function of temperature and pressure has revealed a complex biphase mixture of superconducting FeSe. Based on experimental results we construct a phase diagram where structural behavior and superconducting properties of FeSe are found to be correlated. We show that the superconductivity in FeSe is promoted by a 2D layered pseudo tetragonal structure and strongly suppressed at higher pressure with the formation of a new orthorhombic polymorph characterized by a 3D connectivity. Therefore topological and connectivity properties of FeSe are found to be detrimental for superconductivity to exist. Unambiguous determination of crystal structure of the high pressure polymorph of FeSe ends the long lasting polemics and controversies in the literature.

## Introduction

For cuprates and iron based superconductors the binding of electrons into Cooper pairs is mediated by spin-spin interactions. In the framework of a magnetic pairing model the superconducting critical temperature,  $T_c$ , is enhanced in the case of bi-dimensional structures promoting the coupling between the conduction electrons and the spin fluctuations<sup>1</sup>. However, thermodynamics can spoil a game: even simple solids may show a variety of crystal structures coexisting at the same thermodynamic conditions. Different polymorphic modifications of the same material may vary topologically and, therefore, a modification from 2D layered structure to an environment with a 3D connectivity of magnetic atoms may strongly affect the superconducting properties. In this work, we show that the high pressure dependence of the critical temperature of FeSe is concomitant to a change of the dimensionality of the iron lattice.

The discovery of superconducting transition in the  $\beta$ -FeSe phase in 2008<sup>2</sup> and thereafter in its intercalated derivatives<sup>3,4,5</sup> and other Fe-based systems<sup>6</sup> marked the beginning of the iron age of superconductivity. The  $\beta$ -FeSe phase itself crystallizes in a relatively simple tetragonal PbO-

type structure ( $P4/nmm$  space group, Fig. 1, (a)) and is superconducting below  $T_c = 8-9$  K. The  $T_c$  value can be dramatically increased by intercalating the structure<sup>7</sup> ( $T_c > 40$  K) or by applying high pressure (HP)<sup>8</sup> ( $T_c \sim 37$  K). Moreover, monolayers of the FeSe films were found to become superconducting at 65 K<sup>9</sup> and even above 100 K<sup>10</sup>.

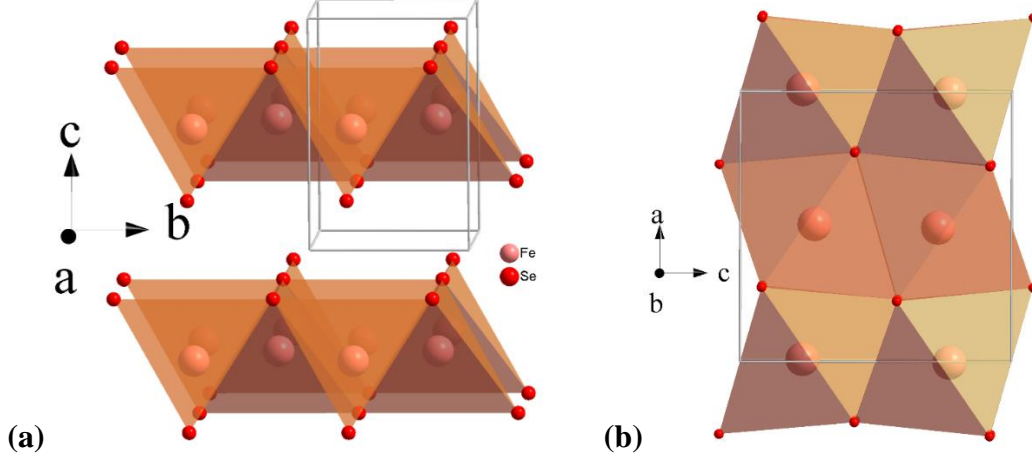


**Figure 1. Low pressure (LP) and high pressure (HP) structures of FeSe** (a) The tetragonal ( $P4/nmm$ ) PbO-type  $\beta$  modification of FeSe composed of layers of edge-shared  $\text{FeSe}_4$  tetrahedra (b) MnP-type ( $Pnma$ ) FeSe phase at high pressure composed of chains of face shared  $\text{FeSe}_6$  octahedra.

Although the  $\beta$ -FeSe phase has a relatively simple crystallographic structure (Fig. 1(a)) and features no long-range magnetic order at low temperature (LT), its behavior as a function of temperature ( $T$ ) and pressure ( $P$ ) is not well understood so far. Below  $\sim 1$  GPa it undergoes a transformation to the orthorhombic ( $Cmma$ ) nematic-type phase around  $T_s = 90$  K<sup>11</sup> with a loss of tetragonal symmetry. Then for pressure above 1 GPa an antiferromagnetic (AFM) phase has been detected by muons spectroscopy<sup>12,13</sup>. It was tracked recently in transport measurements on single crystals<sup>14</sup> which show that this AFM phase exists up to 6 GPa<sup>15</sup> in coexistence with the SC phase. This AFM phase seems to retain the orthorhombic distortion of the  $Cmma$  structure<sup>16</sup>. Such magnetic phase probably competes with superconductivity and affects its pressure dependence of  $T_c$ . The  $T_c$  variation shows at least a double dome feature with a first maximum of 13 K at 0.8-1 GPa followed by a local minimum of 10 K at 1.2-1.5 GPa<sup>17,18</sup>, then an important enhancement<sup>19</sup> up to 34-37 K for  $P = 6-9$  GPa<sup>8,20,21,22</sup> and a saturation or a progressive decrease for pressure up to 10-12 GPa where a structural transition takes place towards a HP phase<sup>21,22</sup>. Two symmetries were proposed for the HP phase (hexagonal<sup>8</sup> or orthorhombic<sup>21</sup>) based on powder X-ray diffraction (XRD) data. However, the unambiguous determination of the crystallographic structure of this HP phase is still lacking, mainly due to the limitation of the X-ray powder diffraction method, even the synchrotron one, in resolving 1D diffraction signals from the disordered (structurally or microstructurally) and likely strained FeSe phase<sup>20,21,22</sup>. Nevertheless, an orthorhombic  $Pnma$  ( $Pbnm$ ) MnP-type model was suggested experimentally and supported by the DFT calculations<sup>23,24</sup>.

Evidently, for such material a high quality crystallographic experiment is a necessary and even decisive ingredient in studying its macroscopic response. Single crystal diffraction data would help to unveil structural details of the HP FeSe polymorph. Since the application of HP strongly increases  $T_c$  in FeSe, establishing the correct structure-property relations could help to

further enhance the superconducting properties of related iron selenides through targeted structural modifications and optimizations.

Here we present high-quality single crystal XRD data collected with synchrotron radiation under hydrostatic conditions in broad range of temperatures (from room temperature (RT) down to 20 K) and pressures (in the 0.2 - 19 GPa range), including the superconducting domain. Presented work allows us to revisit the phase diagram of FeSe and to unambiguously solve the structure of the HP polymorph and uncover the complex biphase nature of the superconducting dome.

## Results and discussion

### Low pressure (LP) ( $P < 6$ GPa) behavior of FeSe

The main focus of the paper is the HP phase of FeSe that appears already below 10 GPa as shown later on. Nevertheless, we have also studied the transformation of the orthorhombic (*Cmma*) LT-LP phase under moderate pressure. At 20 K the ambient pressure orthorhombic distortion of the lattice remains nearly constant up to 6 GPa, i.e. in the AFM phase which gradually appears in the 1-2 GPa range, in agreement with the recent report of Kothapalli *et al.*<sup>16</sup> (see XRD patterns on Fig. 1S and *a-b* axis pressure dependence on Fig. 2S(a)). Interestingly, we detect an anomaly in the *c*-axis and lattice volume at  $1.9 \pm 0.2$  GPa (see Fig. 2S(b)), i.e. in correspondence with the extrapolated curve of  $T_s$  characterizing the nematic transition. This anomaly at 1.9 GPa corresponds also to the onset of the strong enhancement of  $T_c$  and is probably related to changes in hybridization between Se and Fe orbitals as evidenced by the Se height and Fe-Se bond length changes found at 2 GPa and 16 K in the powder XRD study of Margadonna *et al.* [see Fig. 4(a) and (c) in <sup>22</sup>]. At 50 K the *Cmma* orthorhombic distortion disappears at  $1 \pm 0.1$  GPa, and the ambient conditions *P4/nmm* tetragonal phase is recovered, in agreement with the extrapolated pressure dependence of  $T_s$  obtained from resistivity measurements using the same pressure transmitting medium (PTM, helium)<sup>25</sup>. The tetragonal phase is stable in the 1-2 GPa range. Then for higher pressure the lattice distorts again as shown by the broadening of the (04l)-(40l) Bragg peaks (Fig. 1S and Fig. 3S). This corresponds to the onset of the AFM phase detected by muons spectroscopy<sup>13</sup> but not exactly to the onset obtained from other probes like transport measurements<sup>14,15</sup> or Mössbauer spectroscopy (Nuclear forward scattering experiments)<sup>16</sup>. Our results on this LP part of the *P-T* phase diagram are summarized on Fig. 5 with a comparison to the literature.

### LP phase to HP phase transformation mechanism and resolution of the HP structure

We now move to the HP behavior of FeSe, i.e. typically above 6 GPa, and we focus our study on the HP form of FeSe which was assigned in powder XRD studies a hexagonal<sup>8</sup> or orthorhombic<sup>21</sup> symmetries. Our structural model of the HP FeSe modification was obtained from the integrated intensities of the single crystal data collected at 8.1 GPa and RT. It unambiguously corresponds to the orthorhombic MnP-type structure<sup>26</sup> (Table 1, Fig. 1(b)). The experimental reciprocal *h0l* layer of the HP FeSe phase is shown on Fig. 2 and it is consistent with a *Pnma*

symmetry. It features chains of face sharing  $\text{FeSe}_6$  octahedra along the  $a$  axis and, from the first point of view, is not a direct structural derivative of the parent LP tetragonal  $P4/nmm$  FeSe phase.

**Table 1.** Atomic parameters of HP FeSe from single crystal diffraction at 8.1 GPa and 300 K. The structure was solved in the  $Pnma$  space group (equivalent to  $Pbnm$ ),  $a = 5.912(4)$ ,  $b = 3.457(10)$ ,  $c = 5.952(4)$  Å,  $z = 4$ ,  $R_1 = 0.12$  in an anisotropic approach.

Atom	$x$	$y$	$z$	$U_{\text{eq}}$
Fe	0.0069(8)	1/4	0.2259(9)	0.046(3)
Se	0.2237(8)	1/4	0.5786(7)	0.083(4)

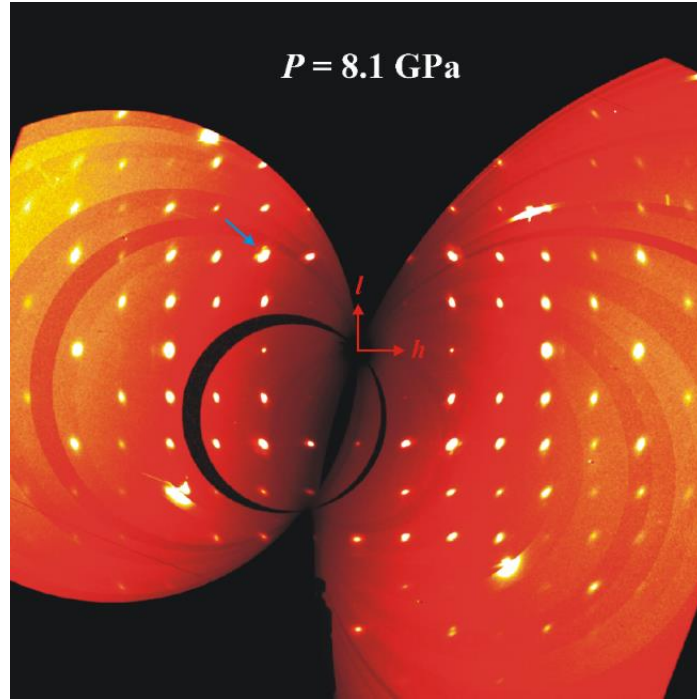


**Figure 2.** The  $h0l$  reciprocal layer of FeSe at 8 GPa from single crystal XRD data. Blue arrow marks a second  $d$ -segregated domain.

The orthorhombic ( $Pnma$ ) MnP-type structure is a slightly distorted hexagonal ( $P6_3/mmc$ ) NiAs-type one<sup>27</sup> that is evidenced, in the case of high-pressure FeSe, by its pseudo-hexagonal lattice ( $a \approx \sqrt{3} \cdot b$ ). A similar conclusion could stem from a comparison of crystal geometry of the ambient-pressure tetragonal ( $P4/nmm$ ) PbO-type structure of FeSe with the LT-LP orthorhombic one ( $Cmma$ ): the latter is a slightly distorted variant of the former. Both distortions (from “tetra” ( $P4/nmm$ ) to “ortho-I” ( $Cmma$ ) and from “hexa” ( $P6_3/mmc$ )-to “ortho-II” ( $Pnma$ )) can be easily identified in symmetry terms:

(i) the phase transformation lowering FeSe crystal symmetry from  $P4/nmm$  ( $Z_p = 2$ ) to  $Cmma$  ( $Z_p = 2$ ) is a proper ferroelastic transition, its mechanism consists of a macroscopic distortion of the tetragonal lattice which is induced by the non-diagonal strain tensor component  $e_6 \equiv e_{xy}$  (irreducible representation  $\Gamma_4^+ \equiv B_{2g}$  from the tetragonal Brillouin Zone (BZ) center)

(ii) displacements in the NiAs-type structure [ $P6_3/mmc$  ( $Z_p = 2$ )] distorting it to the MnP-type one [ $Pnma$  ( $Z_p = 4$ )] represent the eigenvectors for the  $M_2^-$  phonon mode located at the hexagonal BZ face.

Due to the experimentally proved smallness of above distortions, we focus, for the sake of clarity, on the dominating mechanism transforming LP tetragonal (even pseudo-cubic) structure motif to the HP pseudo-hexagonal one. Above remark on non-direct relation between LP and HP structures of FeSe underlines, first, the absence of a group-subgroup link between their space groups. However, such a particularity does not exclude the transformation from the field of regular, symmetry based phenomenological scheme, just assigning it to the reconstructive type<sup>28</sup>. In this case, one should expect non-negligible distortions of the structure, which indeed occur at the transformation (Fig. 3).

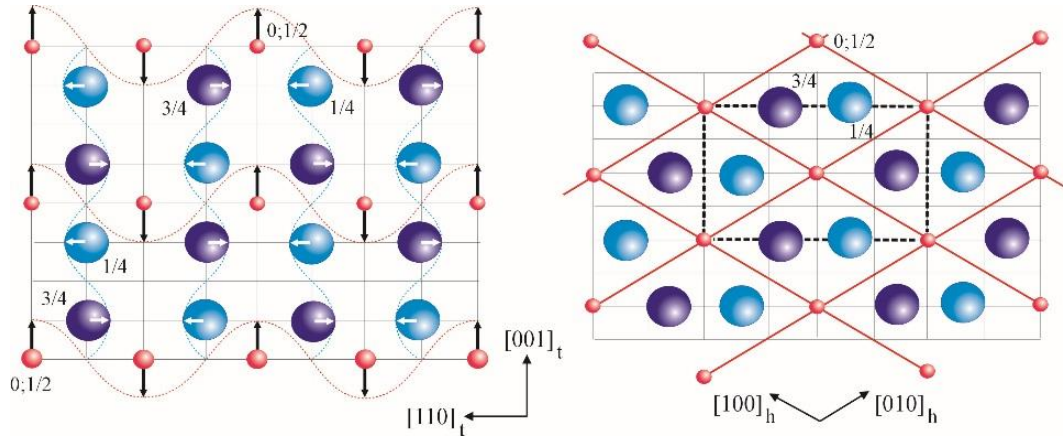


**Figure. 3. Transformation mechanism between LP (PbO-type) and HP (MnP-type) structures of FeSe.** Left panel: displacive  $M_1^t$  phonon field applied to Fe (red spheres) and Se (blue spheres) sublattices. Right panel: result of combined structure distortion by the  $M_1^t$  phonon field and macroscopic  $e_{zz}^t$  strain. Red lines show hexagonal NiAs-type lattice; dashed lines mark the orthorhombic MnP-type structure cell.

We could identify a primary microscopic order parameter (OP) which induces secondary (improper) macroscopic strain. Figure 3 illustrates the OP manifested as antiparallel displacements of both Fe and Se atoms. Despite the perpendicular directions, two sets of the shifts span the same  $M_1^t$  irreducible representation of the  $P4/nmm$  group with the BZ-boundary k-vector  $1/2(b_1^t + b_2^t)$ . In addition to this critical phonon mode, the strain  $e_{zz}^t$  ( $\sim 0.3$ ) is applied to the PbO-type parent structure making its metric hexagonal. The reconstructive character of the transformation justifies its strong discontinuity and, as a consequence, a possible onset of the two-phase coexistence temperature-pressure domain, which was indeed observed in the present

and earlier experiments<sup>8,20,22,23</sup>. It is worth noting that the above mechanism and the corresponding epitaxial relations between LP and HP lattices direct us to the text-book Burgers mechanism of the bcc-hcp transformation<sup>28</sup>; the difference consists in the fact that the latter was suggested for mono-atomic close-packed structures while we deal with their two-atoms derivatives.

### High pressure ( $P > 6$ GPa) behavior of FeSe and its implication on superconductivity

The HP FeSe phase undergoes a rapid microstructural degradation with pressure increase (for 10-12 GPa range see Fig. 4S) even with He as PTM. The degradation includes not only a rotational domain disorder (arching) but also a  $d$ -spacing depending segregation (see also Fig. 2). The latter indicates that the application of pressure induces correlated deviations from the average structure, probably manifested as different local arrangements of the constituting chains of the face sharing FeSe<sub>6</sub> octahedra.

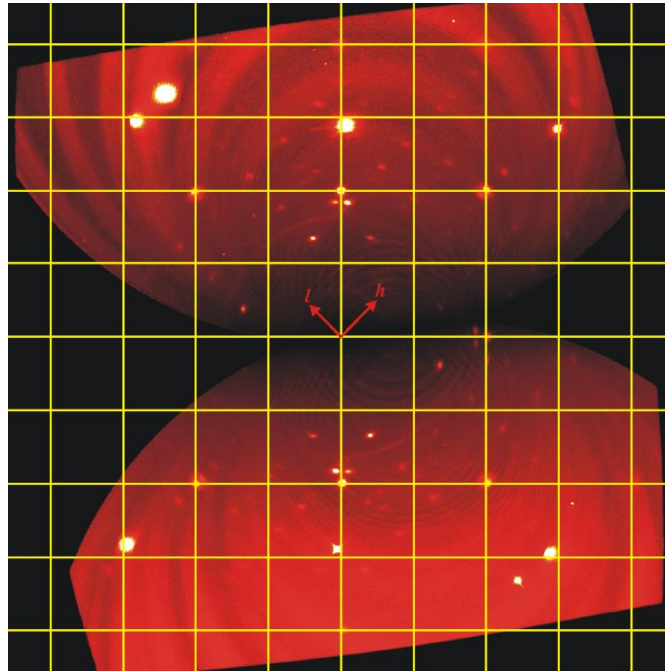


**Figure 4. Coexistence of the HP FeSe phase** (the unit cell is indicated by the red arrows) **and the LP FeSe *Cmma* phase** (the  $hk0$  unit cell grid in the tetragonal setting is represented by yellow lines) **at 20 K and 8 GPa**. Series of the intense peaks (top and bottom, seven in total) not commensurate with the FeSe lattices correspond to diamond reflections from the HP cell.

At 20 K the HP *Pnma* FeSe phase appears between 6.2 and 6.9 GPa. It coexists (Fig. 4, 8 GPa) with the LP *P4/nmm* FeSe phase up to the highest measured pressure of 10 GPa where the HP *Pnma* form is the dominant one. At 50 K the HP *Pnma* is visible at 9.1 GPa and, similarly, coexists with the LT FeSe phase (tetragonal) up to at least 14 GPa. At this temperature the HP *Pnma* phase likely starts to form at around 7 GPa, which corresponds to the interpolation point



between the corresponding transition pressures at RT and 20 K (Fig. 5). However, it may not still be detectable with X-ray radiation do to a small concentration (the corresponding points are colored in cyan on the phase diagram, Fig. 5). Otherwise it would imply a formation of a “pocket” in the “ortho-II” phase around 50 K which would be not rational from a physical point of view. The coexistence of the LP and HP modifications of FeSe in a wide pressure range of at least 4 GPa confirms a first order character of the transformation with a relatively slow kinetics at these temperatures. Indeed, no coexistence of the LP and HP phases is observed at 300 K where the transformation takes place in a pressure point between 6.6 and 8.1 GPa (Fig. 5S). The corresponding  $P,T$  phase diagram for FeSe compares to literature data as follows (Fig. 5). Interestingly, the LP tetragonal/pseudo-tetragonal – HP orthorhombic ( $Pnma$ ) boundary is almost  $T$ -independent.

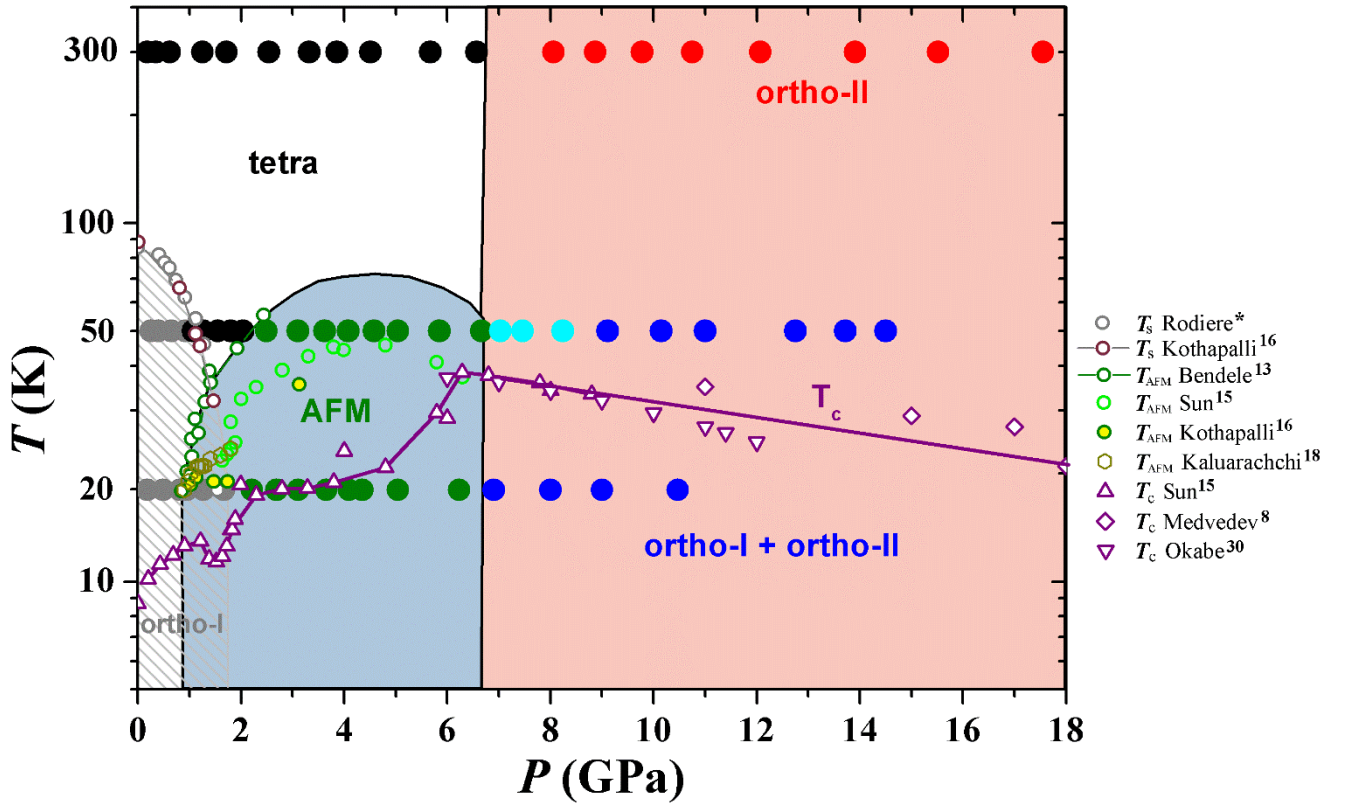


**Figure 5.  $T$ - $P$  phase diagram of FeSe.** Large filled circles at the 20, 50 and 300 K isotherms correspond to the experimental data obtained in this work (black – tetragonal phase, grey – “ortho-I” phase, green – AFM phase, red – “ortho-II” phase, blue – a mixture of “ortho-I” and “ortho-II” phases, cyan – possible onset of the formation of the “ortho-II” phase; \* - our unpublished data based on transport measurements

The LP-HP transition of FeSe was previously studied on powder samples. However, the quality of the experimental diffraction patterns of HP FeSe rapidly degrades with pressure above 6 GPa (see Fig. 4S) that led to controversies in the literature. The formation of the hexagonal

(NiAs-type) FeSe form was suggested at pressures between 8.5 and 12 GPa at RT<sup>20</sup> (He gas as PTM) and above 9 GPa at 16 K<sup>22</sup> (Daphne oil as PTM). However, in the latter studies anomalies in the structural parameters were observed around 8 GPa which coincide with a maximum of  $T_c = 37$  K<sup>22</sup>. Independent magnetization and electrical resistivity measurements on polycrystalline samples with the Daphne 7474 oil (or Daphne 7373) as PTM revealed either a saturation of  $T_c$  for  $P > 3$  GPa<sup>29</sup> or a maximum of  $T_c$  around 6 GPa<sup>30</sup> (value also found recently for FeSe single crystal by Sun *et al.*<sup>15</sup> whereas values in the 6-8 GPa range were reported by<sup>20</sup> and at 7.5 GPa by Miyoshi *et al.*<sup>17</sup> (with argon gas as PTM) on earlier generation of crystals grown in NaCl/KCl flux). Finally, the HP FeSe was identified as an orthorhombic one using powders but with a transition at 12 GPa (He gas as a PTM)<sup>21</sup>. Thus, we conclude that the observed transition pressures were definitively influenced by the PTMs and by the pressure increase rate. Indeed, the latter plays a significant role on the observed behavior for the first-order structural transformations in Cs-intercalated FeSe<sup>31</sup>.

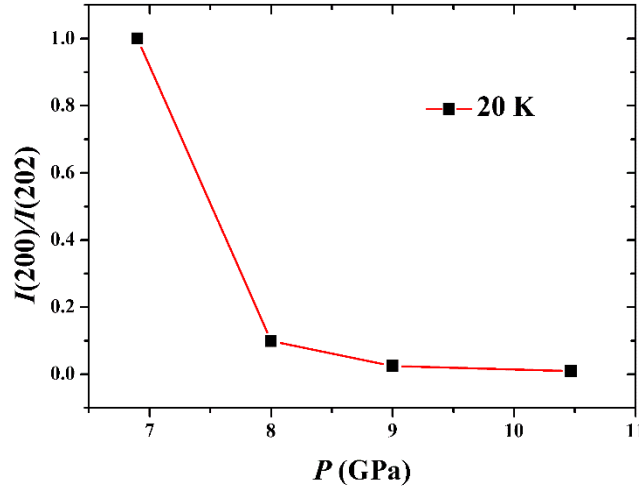


**Figure 6.** Ratios of the intensities of the (200) and (202) peaks of the LP and HP phases of FeSe, respectively, indicating a decrease in the concentration of the LP superconducting phase.

As mentioned above, at 20 and 50 K the LP and HP phases coexist (Fig. 4) up to the highest studied pressures (Fig. 5). However, the LP superconducting *Cmma* pseudotetragonal phase (and the AFM phase) is gradually squeezed out by the HP modification (Fig. 6). The amount of the LP *Cmma* superconducting phase correlates well with the decrease of  $T_c$  in the 6 - 10 GPa range of the superconducting dome for last generation of single crystals<sup>15</sup> (Fig. 5, violet line). Hence the superconducting dome extends over two regions of the phase diagram: one corresponding to the pure pseudo-tetragonal *Cmma* (“ortho-I”) region and the second one to a mixture of the pseudo-tetragonal *Cmma* (“ortho-I”) + HP orthorhombic (“ortho-II”) phases. Therefore we can conclude that the initial LP increase in  $T_c$  is an *intrinsic* effect of the LP “ortho-I” structure while the further decrease in  $T_c$  and the full loss of superconductivity at higher pressures results from the decrease in the *concentration* of the superconducting LP *Cmma* phase (composed of layers of edge-shared FeSe<sub>4</sub> tetrahedra) which is transformed into the HP *Pnma* phase (characterized by a 3D network of face sharing FeSe<sub>6</sub> octahedra). This indicates that



superconductivity must be explained within a single mechanism based on superconducting 2D FeSe layers characteristic of the pseudo-tetragonal structure.

## Conclusions

With the help of X-ray synchrotron radiation and the use of high quality single crystals the nature of the superconducting dome of the FeSe phase diagram was revealed, uncovering relations between topology and macroscopic properties. Within the superconducting dome we observe pressure- and temperature-dependent coexistence of two topologically different phases: a 2D-layered superconducting LP form and a 3D-framework HP form. Pressure increase results in a specific deformation of the layered structure, mainly the decrease in the distance between the FeSe sublayers thus implying an increase in the electron density in the superconducting planes. Further pressure increase above 6 GPa leads to a first order structural transformation of the superconducting phase to a non-superconducting one via nucleation and growth. As a result, the 2D tetragonal FeSe sublayers become uncorrelated and the effective distance between them increases resulting in a decrease in the critical superconducting temperature,  $T_c$ , and the eventual loss of superconductivity. Thus a key parameter for a further enhancement of superconducting properties in the FeSe system is a stabilization of the LP pseudo-tetragonal superconducting phase by a controlled structural tuning, including intercalation and the formation of vacancies.

## Methods

Single crystals of FeSe studied in this work were grown at the Néel Institute (CNRS, Grenoble, France) using a chemical vapor transport (CVT) method based on a mixture of Fe, Se and  $\text{AlCl}_3/\text{KCl}$  chlorides heated in a two-zones furnace. The crystals were fully characterized at ambient pressure<sup>32</sup>.

*P*-dependent single crystal XRD experiments were performed on the ID27 HP beamline at ESRF. The used radiation wavelength was 0.3738 Å, and the data were recorded on a Perkin Elmer flat panel detector. To unambiguously conclude on all of the observed phenomena, a highly hydrostatic PTM has to be used<sup>31</sup>. Therefore He was chosen as a PTM due to its excellent hydrostatic properties up to at least 50 GPa<sup>33</sup>. To cover the pressure range up to 20 GPa diamond anvils with 500 µm culets and rhenium gaskets with 250 µm holes were used. The pressure in the diamond anvil cell was controlled by an automatic pressure drive and was measured using a ruby fluorescence technique<sup>34</sup>. The pressure was changed from 0.1 GPa to a maximum of 19 GPa with a typical step of 1 GPa at the temperatures of 20, 50 and 300 K. We used an in-house developed He cryostat to achieve and control the low temperatures. The experimental diffraction patterns were influenced neither by gasket nor by the ruby spheres up to the highest studied pressures. The experimental single crystal data were integrated and corrected for the absorption with the CrysAlisPro package<sup>35</sup>. Structural solution was obtained with a help of SHELXT program<sup>36</sup>.

## Acknowledgements

The authors thank to S. Bauchau (ESRF), J. Jacobs (ESRF) and P. Strobel (Néel) for technical support.

## Author contributions

V.S., M.R., P.R., P.T. and M.M. conceptualized and designed the research; P.T. grew and characterized the FeSe single crystals; V.S., M.R., P.R., P.T. and M.M. conducted synchrotron X-ray diffraction experiments; V.S., M.R., P.R. and P.T. performed X-ray diffraction data analyses; V.D. and D.C. performed group-subgroup analysis; V.S., M.R., V.D., P.T. prepared figures; V.S. wrote the manuscript with the contributions from all the authors. All authors discussed the results and commented on the paper

## Competing financial interests

The authors declare no competing financial interests

## References

1. Mathur N. D. *et al.* Magnetically mediated superconductivity in heavy fermion compounds. *Nature* **394**, 39-43 (1998).
2. Hsu F.-C. *et al.* Superconductivity in the PbO-type structure  $\alpha$ -FeSe. *Proc. Natl. Acad. Sci. U.S.A.* **105**, 14262-14264 (2008).
3. Guo J. *et al.* Superconductivity in the iron selenide  $K_xFe_2Se_2$  ( $0 \leq x \leq 1.0$ ). *Phys. Rev. B* **82**, 180520 (2010).
4. Krzton-Maziopa A. *et al.* Synthesis and crystal growth of  $Cs_{0.8}(FeSe_{0.98})_2$ : a new iron-based superconductor with  $T_c = 27$  K. *J. Phys.: Condens. Mat.* **23**, 052203 (2011).
5. Wang A. *et al.* Superconductivity at 32 K in single-crystalline  $Rb_xFe_{2-y}Se_2$ . *Phys. Rev. B* **83**, 060512 (2011).
6. Kamihara Y., Watanabe T., Hirano M., Hosono H. Iron-Based Layered Superconductor  $La[O_{1-x}F_x]FeAs$  ( $x = 0.05-0.12$ ) with  $T_c = 26$  K. *J. Am. Chem. Soc.* **130**, 3296-3297 (2008).
7. Krzton-Maziopa A., Svitlyk V., Pomjakushina E., Puzniak R., Conder K. Superconductivity in alkali metal intercalated iron selenides. *J. Phys.: Cond. Mat.* **28**, 293002 (2016).
8. Medvedev S. *et al.* Electronic and magnetic phase diagram of beta- $Fe_{1.01}Se$  with superconductivity at 36.7 K under pressure. *Nat. Mater.* **8**, 630 (2009).
9. He S. *et al.* Phase diagram and electronic indication of high-temperature superconductivity at 65 K in single-layer FeSe films. *Nat. Mater.* **12**, 605-610 (2013).

10. Ge J.-F. *et al.* Superconductivity above 100 K in single-layer FeSe films on doped SrTiO<sub>3</sub>. *Nat. Mater.* **14**, 285-289 (2015).
11. McQueen T. M. *et al.* Tetragonal-to-Orthorhombic Structural Phase Transition at 90 K in the Superconductor Fe<sub>1.01</sub>Se. *Physical Review Letters* **103**, 057002 (2009).
12. Bendele M. *et al.* Pressure Induced Static Magnetic Order in Superconducting FeSe<sub>1-x</sub>. *Phys. Rev. Lett.* **104**, 087003 (2010).
13. Bendele M. *et al.* Coexistence of superconductivity and magnetism in FeSe<sub>1-x</sub> under pressure. *Phys. Rev. B* **85**, 064517 (2012).
14. Terashima T. *et al.* Pressure-Induced Antiferromagnetic Transition and Phase Diagram in FeSe. *J. Phys. Soc. Japan* **84**, 063701 (2015).
15. Sun J. P. *et al.* Dome-shaped magnetic order competing with high-temperature superconductivity at high pressures in FeSe. *Nat. Commun.* **7**, 12146 (2016).
16. Kothapalli K. *et al.* Strong cooperative coupling of pressure-induced magnetic order and nematicity in FeSe. *Nat. Commun.* **7**, 12728 (2016).
17. Miyoshi K. *et al.* Enhanced Superconductivity on the Tetragonal Lattice in FeSe under Hydrostatic Pressure. *J. Phys. Soc. Japan* **83**, 013702 (2014).
18. Kaluarachchi U. S. *et al.* Nonmonotonic pressure evolution of the upper critical field in superconducting FeSe. *Phys. Rev. B* **93**, 064503 (2016).
19. Mizuguchi Y., Tomioka F., Tsuda S., Yamaguchi T., Takano Y. Superconductivity at 27 K in tetragonal FeSe under high pressure. *Appl. Phys. Lett.* **93**, 152505 (2008).
20. Braithwaite D. *et al.* Superconducting and normal phases of FeSe single crystals at high pressure. *J. Phys.: Cond. Matt.* **21**, 232202 (2009).
21. Garbarino G. *et al.* High-temperature superconductivity ( $T_c$  onset at 34 K) in the high-pressure orthorhombic phase of FeSe. *Europhys. Lett.* **86**, 27001 (2009).
22. Margadonna S. *et al.* Pressure evolution of the low-temperature crystal structure and bonding of the superconductor FeSe ( $T_c = 37$  K). *Phys. Rev. B* **80**, 064506 (2009).
23. Kumar R. S. *et al.* Crystal and Electronic Structure of FeSe at High Pressure and Low Temperature. *J. Phys. Chem. B* **114**, 12597-12606 (2010).
24. Naghavi S. S., Stanislav C., Claudia F. The role of correlations in the high-pressure phase of FeSe. *J. Phys.: Cond. Matt.* **23**, 205601 (2011).
25. Knöner S. *et al.* Resistivity and magnetoresistance of FeSe single crystals under helium-gas pressure. *Phys. Rev. B* **91**, 174510 (2015).
26. Rundqvist S. Phosphides of the B31 (MnP) structure type *Acta Chem. Scand.* **16**, 287-292 (1962).

27. Franzen H. F., Haas C., Jellinek F. Phase transitions between NiAs- and MnP-type phases. *Phys. Rev. B* **10**, 1248-1251 (1974).
28. Toledano P., Dmitriev V. Reconstructive Phase Transitions in Crystals and Quasicrystals. World Scientific (1996).
29. Miyoshi K., Takaichi Y., Mutou E., Fujiwara K., Takeuchi J. Anomalous Pressure Dependence of the Superconducting Transition Temperature in FeSe<sub>1-x</sub> Studied by DC Magnetic Measurements. *J. Phys. Soc. Japan* **78**, 093703 (2009).
30. Okabe H., Takeshita N., Horigane K., Muranaka T., Akimitsu J. Pressure-induced high-T<sub>c</sub> superconducting phase in FeSe: Correlation between anion height and T<sub>c</sub>. *Phys. Rev. B* **81**, 205119 (2010).
31. Svitlyk V. *et al.* Compressibility and pressure-induced disorder in superconducting phase-separated Cs<sub>0.72</sub>Fe<sub>1.57</sub>Se<sub>2</sub>. *Phys. Rev. B* **89**, 144106 (2014).
32. Karlsson S. *et al.* Study of high-quality superconducting FeSe single crystals: crossover in electronic transport from a metallic to an activated regime above 350 K. *Supercond. Sci. Technol.* **28**, 105009 (2015).
33. Takemura K. Evaluation of the hydrostaticity of a helium-pressure medium with powder X-ray diffraction techniques. *J. Appl. Phys.* **89**, 662-668 (2001).
34. Forman R. A., Piermarini G. J., Barnett J. D., Block S. Pressure Measurement Made by the Utilization of Ruby Sharp-Line Luminescence. *Science* **176**, 284-285 (1972).
35. Rigaku Oxford Diffraction, CrysAlisPro Software system, version 1.171.38.41, Rigaku Corporation, Oxford, UK (2015).
36. Sheldrick G. SHELXT - Integrated space-group and crystal-structure determination. *Acta Crystallogr. A* **71**, 3-8 (2015).